AD_____

GRANT NO: DAMD17-94-J-4058

Original contains color plates: All DTIC reproductions will be in black and white

TITLE: Development of a High Resolution Digital Mammography System

PRINCIPAL INVESTIGATOR: James K. Walker, Ph.D.
Zhenxue Jing

CONTRACTING ORGANIZATION: University of Florida
Gainesville, Florida 32611

REPORT DATE: 12 Sep 95

TYPE OF REPORT: Annual

PREPARED FOR: U.S. Army Medical Research and Materiel Command
Fort Detrick, Maryland 21702-5012

DISTRIBUTION STATEMENT: Approved for public release; distribution unlimited

REPORT DOCUMENTATION PAGE

Form Approved
OMB No. 0704-0188

1. AGENCY USE ONLY (Leave blank)	2. REPORT DATE	3. REPORT TYPE AND DATES COVERED
	12 Sept 95	Annual 15 Aug 94 - 14 Aug 95

4. TITLE AND SUBTITLE
Development of a High Resolution Digital Mammography System

5. FUNDING NUMBERS
DAMD17-94-J-4058

6. AUTHOR(S)
James K. Walker, Ph.D.
Zhenxue Jing

7. PERFORMING ORGANIZATION NAME(S) AND ADDRESS(ES)
University of Florida
Gainsville, Florida 32611

8. PERFORMING ORGANIZATION REPORT NUMBER

9. SPONSORING/MONITORING AGENCY NAME(S) AND ADDRESS(ES)
U.S. Army Medical Research and Materiel Command
Fort Detrick, Maryland 21702-5012

10. SPONSORING/MONITORING AGENCY REPORT NUMBER

11. SUPPLEMENTARY NOTES

12a. DISTRIBUTION/AVAILABILITY STATEMENT
Approved for public release; distribution unlimited

12b. DISTRIBUTION CODE

13. ABSTRACT *(Maximum 200 words)*

The primary goal of this predoctoral fellowship research project is to develop a plastic scintillating fiber plate (SFP) to replace the phosphor screen as currently being used in the phosphor-CCD scanning slot digital mammography system.

We have (1) developed one 2 cm thick, parallax corrected, slot shaped SFP module with 7.5% tin loaded into the scintillating fiber core material. Methods to enhance the scintillation light generation and collection were used. Experiment to measure the scintillation output from the SFP is being conducted; (2) built a CCD camera and readout electronics. A measured total thermal and readout noise level of 100 e^- rms has been achieved at 2 MHz readout rate and 28°C. (3) set up a testing system which includes a mammography x-ray unit, a high speed image grabber, and a computer controlled linear scanning table; (4) studied the scatter effect using Monte-Carlo methods. An airgap method is found to be efficient to remove the scattered radiation.

Our preliminary results indicated that high detective quantum efficiency (> 70%) is achievable with the scanning slot x-ray imaging detector being integrated at present.

14. SUBJECT TERMS	15. NUMBER OF PAGES
Digital Mammography, Scintillating Fiber, TDI-CCD, DQE, Scattered Radiation	23
	16. PRICE CODE

17. SECURITY CLASSIFICATION OF REPORT	18. SECURITY CLASSIFICATION OF THIS PAGE	19. SECURITY CLASSIFICATION OF ABSTRACT	20. LIMITATION OF ABSTRACT
Unclassified	Unclassified	Unclassified	Unlimited

NSN 7540-01-280-5500

Standard Form 298 (Rev. 2-89)
Prescribed by ANSI Std. Z39-18
298-102

FOREWORD

Opinions, interpretations, conclusions and recommendations are those of the author and are not necessarily endorsed by the US Army.

____ Where copyrighted material is quoted, permission has been obtained to use such material.

____ Where material from documents designated for limited distribution is quoted, permission has been obtained to use the material.

____ Citations of commercial organizations and trade names in this report do not constitute an official Department of Army endorsement or approval of the products or services of these organizations.

____ In conducting research using animals, the investigator(s) adhered to the "Guide for the Care and Use of Laboratory Animals," prepared by the Committee on Care and Use of Laboratory Animals of the Institute of Laboratory Resources, National Research Council (NIH Publication No. 86-23, Revised 1985).

____ For the protection of human subjects, the investigator(s) adhered to policies of applicable Federal Law 45 CFR 46.

____ In conducting research utilizing recombinant DNA technology, the investigator(s) adhered to current guidelines promulgated by the National Institutes of Health.

____ In the conduct of research utilizing recombinant DNA, the investigator(s) adhered to the NIH Guidelines for Research Involving Recombinant DNA Molecules.

____ In the conduct of research involving hazardous organisms, the investigator(s) adhered to the CDC-NIH Guide for Biosafety in Microbiological and Biomedical Laboratories.

James K Walker 9/12/95

PI - Signature Date

TABLE OF CONTENTS

INTRODUCTION

Background

Breast cancer is the most common malignant neoplasm and the leading cause of cancer deaths for women in the United States. Clinical requirements for early detection of breast cancer include detection of subtle architectural distortion, masses with densities very close to normal tissue and skin thickening. It is also important to detect microcalcifications which are specks of calcium hydroxyapatite [$Ca_5(PO_4)_3OH$] and which may have diameters as small as 0.1 mm.

Screen-film mammography is the only reliable means of detecting nonpalpable cancers at present. Early detection with screening mammography has been shown to significantly reduce breast cancer mortality rates for women over age 50. However, there are four major technical limitations which reduce the accuracy of screen-film mammography: (1) The shape of the film's characteristic curve necessitates a compromise between display contrast and exposure latitude [1]. (2) The presence of film granularity significantly reduces the signal-to-noise ratio (SNR) of the displayed image, and especially degrades the system's ability to demonstrate microcalcification [2,3]. (3) Scattered radiation greatly reduces the displayed contrast and SNR. Conventional scatter rejection techniques using grids can lead to a factor of 2 to 4 increase in mean glandular dose [4-8]. (4) There is a tradeoff between screen absorption efficiency and spatial resolution [2]. (5) It is difficult to retrieve old mammograms for comparison due to the massive archive of hardcopy films.

Digital mammography has the potential to overcome the limitations of screen-film mammography and to improve the sensitivity and specificity of breast cancer detection. The decoupling of image acquisition, storage, and display stages allows the optimization of each stage. Digital mammography also provides additional benefits including digital archive, computed assisted diagnosis and teleradiology.

The technical requirements for digital mammography are extremely demanding. A number of ROC studies [9,10] have been performed to study the resolution requirement for digital mammography by digitizing screen-film mammograms with ~ 100 μm pixel size. Almost all these studies suggested that differentiation of benign from malignant cases always decreased because of the large pixel sizes used. The ROC study by Chan et al [11] demonstrated that very high spatial resolution (a pixel size of 0.035 mm x 0.035 mm or smaller) will be required for digital mammography in order to capture the very subtle microcalcifications detectable on screen-film mammograms.

The dynamic range requirement of a digital mammography system depends on the x-ray energy spectra, scattered radiation, breast thickness and composition. For both molybdenum (Mo) target and tungsten (W) target spectra, a number of phantom and clinical studies have shown that the maximum intensity to minimum intensity ratio in the distribution of x-ray exposure transmitted by the breast ranges from 10 to about 400 without and with the presence of scattered radiation [12,13]. Any digital mammography

system with scatter rejection should have a linear response over 400:1 of maximum to minimum x-ray transmission ratio.

Current Approaches to Digital Mammography

To realize the benefits of digital mammography, x-ray imaging detector with appropriate characteristics must be developed. Various configurations for the acquisition of digital mammograms have been proposed [1,14-17]: (a) different detector geometry such as area, point, line, and slot, (b) different x-ray detectors such as digitized film, photostimulable phosphor, amorphous selenium, and traditional phosphor screens optically coupled to charge-coupled devices (CCDs).

Point and line detector geometries are almost impossible to use because of the extremely high x-ray tube loading and long imaging time which may require. Computed radiography (CR) systems using photostimulable phosphor have limited applications because of its low resolution (< 10 lp/mm) performance. CR systems based on selenium detector has the potential to achieve very high detective quantum efficiency (DQE), and is being evaluated clinically for thoracic imaging with limiting detector resolution of less than 3 lp/mm [18,19]. It is questionable that very high spatial resolution will be obtained with selenium detectors. Also, CR systems using selenium detector may be too expensive to compete with screen-film mammography for general breast cancer screening.

At present, the most promising detector is shown to be a rare-earth phosphor slot screen coupled by tapered fiber optic image guide to CCDs, which are operated in the time-delayed integration (TDI) mode while the slot detector is scanned [1,17]. Zero spatial frequency detective quantum efficiency (DQE) of a phosphor-CCD system is measured to be ~ 60%, this is to be compared to that of ~ 30% for screen-film combinations [20]. However, there are intrinsic limitations of this system which mainly stem from the use of phosphor: (1) Using a phosphor coupled to a CCD via a fiber optic image guide will inevitably reduce the spatial resolution compared to modern screen-film mammography, for which a single emulsion film is used in combination with a single back-intensifying screen. (2) The phosphor screen is made of Gd_2O_2S:Tb. The afterglow (slow scintillation decaying component) nature of this phosphor will likely prevent its use for fast scanning applications [21]. The image acquisition time for each detector pixel in TDI mode scanning is about 1 msec (50 μm detector moving at 5 cm/sec to cover 20 cm length in 4 seconds). During the 1 msec exposure time, Gd_2O_2S:Tb phosphor emits only 47% of its total scintillation light. The rest of the scintillation light will spread to adjacent pixels while the charges in the CCD pixels are integrated along the entire TDI column. This will significantly reduce image contrast and detector modulation transfer function (MTF) at all spatial frequencies.

In summary, the reported limiting spatial resolutions are less than 10 lp/mm for most digital mammographic imaging systems being developed.

Purpose Of The Present Work And The Method Of Approach

The primary goal of this predoctoral fellowship research project is to develop a plastic scintillating fiber plate (SFP) and methods to maximize its scintillation light generation and output to replace conventional phosphor screens as currently being used in the phosphor-CCD slot scanning digital mammography system. A prototype scanning slot digital mammography detector based on this SFP shall be constructed, and its imaging performance shall be evaluated.

We have shown that the use of a plastic scintillating fiber plate (SFP) as the x-ray-to-light converter permits a better compromise between spatial resolution and x-ray absorption efficiency than traditional phosphor screens [22]. An x-ray imaging SFP is an array of scintillating fibers aligned together with their axis parallel to the direction of incident x-ray beams. SFPs incorporate scintillation material within each fiber core. A fraction of the light from scintillation is trapped in the fiber where it is generated, preserving the spatial resolution by minimizing light dispersion within the plate as shown in Figure 1. A thicker plate can therefore be used to increase the x-ray absorption efficiency without degrading the spatial resolution.

In order to increase the x-ray absorption efficiency and energy conversion efficiency, we proposed to incorporating a small amount of tin (~ 10% by weight) into the core of plastic microfibers. To improve the scintillation light output from the SFP, we also proposed to use very low refractive index cladding on each microfiber core. By careful choice of scintillating dyes, we were able to double the conversion efficiency to 6% with polymer based scintillator.

Other superior imaging characteristics of the SFP include: (1) In phosphor screens, there are sources of non-Poisson noise related to the scintillation efficiency which causes degradation of screen DQE. Contrary to that case, the proposed SFP is immune to this noise, i.e., the scintillation light output is independent of the x-ray conversion location within the SFP, as can be seen in Figure 1. (2) The scintillation light decay time is only a few nano-second. This guarantees negligible afterglow effect and no degradation of temporal MTF when used in fast scanning applications.

One of the potential benefits of a digital mammography system is that it will promote digital image processing and other CAD methods, which have the potential to reduce the screening load and improve the diagnostic accuracy by reducing the number of false negative (missed) diagnosis. CAD schemes are ultimate goal in mammography. However, its success depends primarily on the availability of high quality primary digital mammograms. The study by Chan, et al indicated that the accuracy in the detection of microcalcifications using a CAD method decreases significantly as the pixel sizes increases from 35 μm to 70 μm [11]. By applying wavelet based image processing algorithms to digitized mammograms, Clark, et al have also shown that clusters of microcalcifications and their morphologic aspects in the processed mammograms were clearly presented when screen-film images were digitized with 35 μm pixel size, but very difficult to be identified in the original mammograms and processed mammograms with

pixel size of 100 μm [23]. The proposed digital mammography system is being developed with limiting spatial resolution of 15 lp/mm. The combination of this high performance digital mammography system and appropriate CAD methods will refine the perception of mammographic features (including lesions, masses, and microcalcifications) and greatly improve the sensitivity and specificity in the early detection of breast cancers.

BODY

PLASTIC SCINTILLATING FIBER PLATE

A schematic of the prototype scintillating fiber plate (SFP) based digital mammography detector is shown in Figure 2. The 5 cm long, 0.8 cm wide slot shaped detector is formed by two modules. Each module is composed of a 2 cm thick SFP, a microfiber fiber image guide with 1:1 input to output ratio, and a front-illuminated 1100 x 330 pixels CCD with 24 μm pixel size. The image guide is composed of the same fibers used to make the SFP, and is actually a continuation of the SFP. The bend in the image guide ensures that the CCDs are not directly exposed to the primary x-ray field.

The properties of the plastic scintillating fibers used for this application is shown in the following table.

Microfiber	Core		Cladding	
Diameter	Material	Refractive index	Material	Refractive index
20 μm	Polystyrene + 7.5% tin	1.59	Fluorinated Polymer	1.35

Scintillation light produced by the ionizing photoelectron is guided by internal reflections along the fiber. The fraction F, of scintillation light which is transmitted within the fiber is given by

$$F = \frac{1}{2}\left(1 - \frac{n_{clad}}{n_{core}}\right) = 7.5\%$$

where n_{core} and n_{clad} are the refractive indexes of the optical fiber cladding and core materials. Due to the use of Fluorinated Polymer as the cladding in our plastic scintillating fibers, this fraction , F, is increased to 7.5% compared to the fraction of 3% for typical plastic optic fibers.

We proposed to use amorphous fluoropolymer AF 1600 as the cladding material which theoretically shall provide a 9% scintillation light collection efficiency. During the progress of this project, we found that properties of Fluorinated Polymer cladding and tin loaded polymer core are matched better than AF 1600 and the tin loaded polymer core. The measured numerical apertures are very close for tin loaded fibers cladded with Fluorinated Polymer and AF 1600. Because Fluorinated Polymer is much cheaper than AF 1600. We decided to use Fluorinated Polymer as the cladding material for fibers used to develop the detector for mammography.

Because of the low Z properties of plastic material, a large fraction of interactions between incident x-ray photons and the fiber material are Compton scattering. Scattered x-ray photons carry a large portion of incident energy away from the first interaction site and may register false spatial information at remote sites within the SFP. This will decrease image resolution and reduce the signal to noise ratio. To convert the incident x-ray photon energy into useful image information more efficiently, we have successfully loaded 7.5% by weight of tin element into plastic scintillating fiber core. The scintillation light loss due to quenching is measured to be less than 10%. At mammographic x-ray energy range, this will increase the stopping power significantly within a short fiber length and also shift the x-ray interactions with the SFP to be photoelectric effect dominant.

One potential problem associated with a tin loaded SFP is the scintillation light contribution from the absorption of characteristic x-rays generated within the SFP. Since characteristic x-rays (K and/or L x-rays) are emitted almost isotropically in all directions, their reabsorption in the detector leads to loss of spatial resolution [24-27]. For mammography, the K and L x-rays of tin (K-edge at 29.20 keV, and $E_L \cong 4$ keV) are encountered [28-30]. When the incident x-ray energy is less than the tin K-edge, the fraction of energy carried by interacting photons that is transferred to L x-rays is given by:

$$L(E) = \frac{\left(\mu/\rho\right)_L E_L}{\left(\mu/\rho\right)_T E}\omega_L$$

where $(\mu/\rho)_L$ is the mass attenuation coefficient for L-shell photoelectric interactions and $(\mu/\rho)_T$ is the total mass attenuation coefficient. E is the incident photon energy, E_L is the energy of the L x-ray photon, and ω_L is the L-shell fluorescent yield. The x-ray attenuation characteristics and L(E) for the 7.5% tin loaded plastic scintillating fiber at 20 keV incident x-ray energy are listed in the table below.

	Density (g/cm^3)	$(\mu/\rho)_L$ (cm^2/g)	$(\mu/\rho)_T$ (cm^2/g)	ω_L (%)	E_L (keV)	L(20 keV) (%)
7.5% Sn Load SFP	1.13	1.70	1.87	6.65	3.8	1.15

It is seen that only about 1% of the incident photon energy is transferred to the L x-ray energy. Since the fraction of x-ray photons with energy greater than 30 keV is either zero or very small in typical mammography x-ray energy spectra, the effect of characteristic x-ray emission and/or reabsorption within the SFP shall be minimum.

We proposed to load 10% tin by weight into the fiber core. Although we have produced plastic scintillators with 10% tin by weight, we found from measurements that loading of 7.5% tin by weight generates more scintillation light than the loading of 10% tin by weight. In fact, the scintillation light generation increases as the fraction of tin loading increasing from 0% to about 7.5% by weight, but decreases as the fraction of tin loading increasing further. This is the result of two opposite processes: loading tin improves the

x-ray energy absorption within the fiber core, but decreases the scintillation light output due to the quenching effect. 7.5% tin by weight is an optimized loading fraction for this application.

To better illustrate the advantage of our SFP, a drawing of the parallax corrected SFP is shown in Figure 3.

The calculated quantum absorption efficiency of this 2 cm thick, 7.5% tin loaded SFP is shown in Figure 4. This absorption efficiency is superior to those of the mostly used Min-R screens for mammography [20].

CCD CAMERA AND READOUT ELECTRONICS

The specifications of the CCDs used (KAF-0360, Eastman Kodak Company) are shown in the table below.

Size	26.4 mm x 7.92 mm
Pixel size	24 μm x 24 μm
Array	1100 x 330
Full Well Capacity	200,000 electrons
Dark Current @25°C	1080 e^-/pixel/second
Readout Noise @1 MHz @25°C	50 e^- rms/pixel (see note)
Amplifier Sensitivity	10 μV/e^-
Quantum Efficiency	average ~40% for the light output from SFP

note: correlated double sampling is assumed

Images will be acquired by scanning a fan x-ray beam and the slot detector in a direction parallel to the short dimension of the detector (7.92 mm, 330 pixels). To allow a smooth mechanical motion, the CCDs are operated in the time-delayed integration (TDI) mode. Each CCD is capable of bi-directional TDI mode operation, and operated in Multi-Pinned-Phasing (MPP) mode of operation to reduce CCD pixel dark current generation.

TDI is based on the concept of taking multiple exposure of the same object [31,32]. In TDI operation, as the detector is moved across the breast at constant speed the charge collected in each pixel of the CCD is shifted down its column at the same speed as that of the scan but in the opposite direction. This allows the charge generated in one portion of the image to integrate in the detector (CCD) during image acquisition, eventually providing a signal 330 times larger than that accumulated in any individual pixel. The charge packets in each row (1024 out of 1100 pixels) are readout at 2 MHz when they reach the last row (also called the serial register) in the CCD, a line of the final image is then formed. The CCD readout noise only contributes once to the integrated charge signal.

A modular, low noise, fast readout CCD camera has been developed for this project. This CCD camera is designed to be operated at ambient temperature. The

output from a CCD is amplified and then digitized at 2 MHz with a 14 bit analog-to-digital converter (ADC) located in the camera head. In our prototype detector, the two CCDs are readout in parallel in order to maintain the 5 cm/second scanning speed. Correlated double sampling (CDS) [31] is implemented to reduce the effect of CCD reset noise. The image data is then captured by a fast image grabber developed by Imaging Technology Inc. This grabber is capable of acquiring image data at 35 MByte/s, which can handle the simultaneous output from eight of our camera modules (2 MHz x 2Byste x 8 = 32 MByte/s).

Fixed pattern noise (FPN) will be removed by a simple algorithm which is being implemented on line during the scanning process in the camera readout hardware. Before image acquisition, two line correction tables (8800 pixels/line) will be recorded first. A dark correction table I_d is generated by scanning the detector in its normal TDI operation mode for the entire image area without x-ray exposure to the detector. The ith pixel in the dark correction table is calculated from averaging the pixel intensity over the total pixels in the ith column along the TDI direction. A flat field correction table I_f is obtained in the same way with high exposure to the detector so that the x-ray intensity fluctuation is negligible. During image acquisition, each line of the original image $I_{o,j}$ will be corrected on line by the following algorithm [32,33]

$$I_{c,j} = F \times \frac{I_{o,j} - I_d}{I_f - I_d}$$

where $I_{c,j}$ is the jth line of the corrected image, F is an arbitrary value. The x-ray quantum noise in the corrected pixel data will equal to that in the uncorrected pixel data because the averaging process and high x-ray exposure involved to obtain the correction tables.

EXPERIMENTAL SETUP

The imaging performance of the prototype scanning slot digital mammography detector will be tested by fixing the x-ray tube and detector at 60 cm distance, while testing phantoms are moved by a linear motion table in the horizontal direction from one side of the detector to the other side. Testing phantoms are mounted on a 5 mm acrylic plate, which is supported by the linear motion table. The x-ray generator is capable of operating continuously for 4 seconds with uniform output. Phantom images will be obtained using a Mo-anode x-ray tube with an 0.3 mm focal spot size and 30 μm Mo filter. Figure 5 illustrates the functional diagram of this experiment setup.

The synchronization between the phantom movement and CCD pixel charge shift is the critical circuit that permits the TDI mode of imaging operation [31]. A synchronization signal is required for each line to shift the integrating image one pixel in the opposite direction of the moving phantom. In our experimental setup, an electronic pulse signal which is related to the phantom movement was obtained through the application of a linear encoder to the linear table. This signal was modified as the application demands and sent to the CCD camera so that the charge shifting is slaved to the object movement.

The linear encoder has a resolution of 1 μm, i.e., the encoder can produce one electronic pulse every 1 μm of object travel. The synchronization signal was generated by a timing circuit which counts the number of encoder outputs at an 24 pulses interval (24 μm linear movement). In this way, any speed variation in the object motion is automatically coupled to CCD clocking which moves the charge. Spatial resolution degradation due to velocity mismatch between phantom and CCD pixel charge movement is minimized.

REJECTION OF SCATTERED RADIATION

The absorption of scattered photons from breast by the x-ray detector degrades image contrast and increases the noise level in the breast images. This makes the perception of microcalcification and small differences in tissue density more difficult. The amount of degradation on contrast and SNR depends upon the ratio of scattered to primary photons absorbed by the detector, S/P. S/P is a function of x-ray energy, x-ray field size, detector size, breast thickness, and breast composition.

By collimating the x-ray field to the sensitive area of the slot detector, scattered radiation can be effectively reduced [34]. To study the amount of scattered radiation encountered in scanning slot digital mammography, we computed the S/Ps using Monte Carlo method under the proposed imaging geometry [35]. X-ray energy spectra were taken from the measured data by Fewell et al [36]. Three breast compositions were simulated consisting of 99.9% adipose + 0.1% glandular tissues (adipose breast), 50% adipose + 50% glandular tissues (average breast), and 0.1% adipose + 99.9% glandular tissues (glandular breast) [37]. The error on each value of S/P due to statistical fluctuations is less than 1%.

Figure 6 shows the calculated S/P values as a function of breast thickness for the three breast compositions for a typical mammography x-ray energy spectrum. The fact that, when there is no airgap between the compressed breast and slot detector, S/P ranges from 0.15 to 0.36 indicated that a factor of 1.15 to 1.36 in the reduction of image contrast due to scattered radiation. Because of the existence of this relatively large amount of scattered radiation level for the scanning slot digital mammography system, one paper was published in medical physics which investigated the use of anti-scattering grid [38]. We have found in our simulation study that the use of a 3 cm airgap significantly reduces the S/P, as also shown in Figure 6. The increased breast dose from this small airgap is almost negligible.

In screen-film mammography, mammographic grids transmit 60% to 75% of the primary x-rays and absorb 75% to 85% of the scatter. This results in 2 to 3 times increase in breast dose. The resulted S/P ranges from about 10% to 20% for breast thickness from 3 cm to 8 cm [7,8].

We concluded that airgap technique is much more efficient than grids to reduce the amount of scattered radiation in scanning slot digital mammography. An optimized

airgap will be determined from both simulations and experiments which will be performed using the prototype imaging system.

CONCLUSION

To summarize our progress after one year of work, we have:

(1) successfully developed one plastic scintillating fiber slot module (SFP + bended image guide) with 7.5% tin loaded into the scintillating fiber core material. Using fluorinated polymer, we increased the scintillation light collection efficiency from typically 3% to 7.5%. The fiber core material also consists of a special developed scintillating dye (Nanoptics Inc.) which has a measured energy conversion efficiency of 4.5% from x-ray photon energy to visible photon energy, a 1.5 times improvement compared to most plastic scintillators. Experiment to measure the scintillation light output from the SFP is being conducted.

These achievements are critical in realizing the goals of this research. The amount of scintillation light output from SFP determines, to a large extent, the ultimate detector DQE. From the above measurement, we estimate that the detector zero spatial frequency DQE is greater than 70% for typical detector exposure level (> 3 mR) encountered in mammography.

(2) set up the testing system to perform the imaging performance measurements at Nanoptics, Inc. This setup includes a mammography x-ray unit (Senograph 500t), a modified PC based high speed PCI bus frame grabber, and a linear scanning table with a computer controlled motion controller which generates the synchronization signals for CCD camera electronics.

The synchronization between object motion and CCD charge shifting is very important to achieve the goal of 15 lp/mm detector limiting spatial resolution. Also it is critical to align the CCD columns to the scanning direction. In the proposed imaging system, the fast scanning application requires the large amount of digitized image data to be acquired and stored in very short time. The success in setting up these components allows the prototype SFP detector imaging performance to be evaluated accurately.

(3) built the CCD camera readout electronics. A measured total thermal and readout noise level of 100 e^- rms has been achieved at 2 MHz readout rate and 28°C. The CCD camera and readout electronics are being optimized for lower noise performance at present.

This is another critical component in the prototype scanning slot digital mammography system which determines the detector DQE and the system linear dynamic range. Our goal is to obtain a total thermal and readout noise level of ~ 50 e^- rms at 2 MHz readout rate and 25°C.

(4) studied the effect of scattered radiation using Monte-Carlo methods. It is found that the amount of scattered radiation present in the prototype imaging system is significant. An airgap method is found to be efficient to remove the scattered radiation. This technique will be employed in the digital mammography system being developed.

Figure 7 shows a photograph of one SFP module, two CCDs, and the frame grabber. Figure 8 is a photograph of the mammography x-ray unit and the linear scanning table. Figure 9 (a) shows a photograph of the CCD camera electronics and one CCD module. Figure 9 (b) also shows one ADC module and the camera readout unit. It is noted that the developed CCD camera is capable of support eight CCD and associated modules which will form a CCD camera for a full scale scanning slot digital mammography system.

It is anticipated that breast phantom images acquired using this two SFP-CCD module prototype unit will be shown in late November at the 1995 RSNA annual meeting in Chicago.

ILLUSTRATIONS

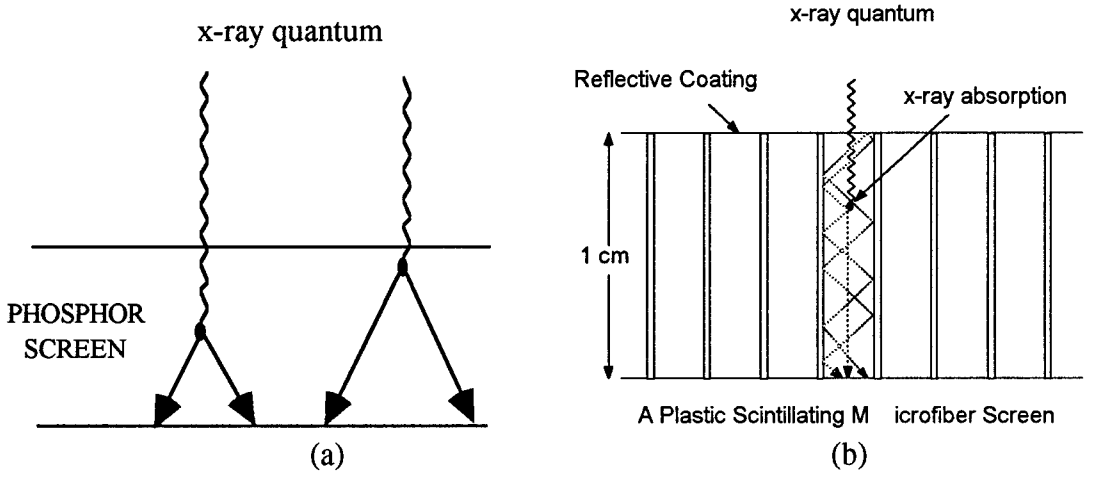

Figure 1. Light dispersion in (a) a phosphor screen, (b) a plastic scintillating fiber plate

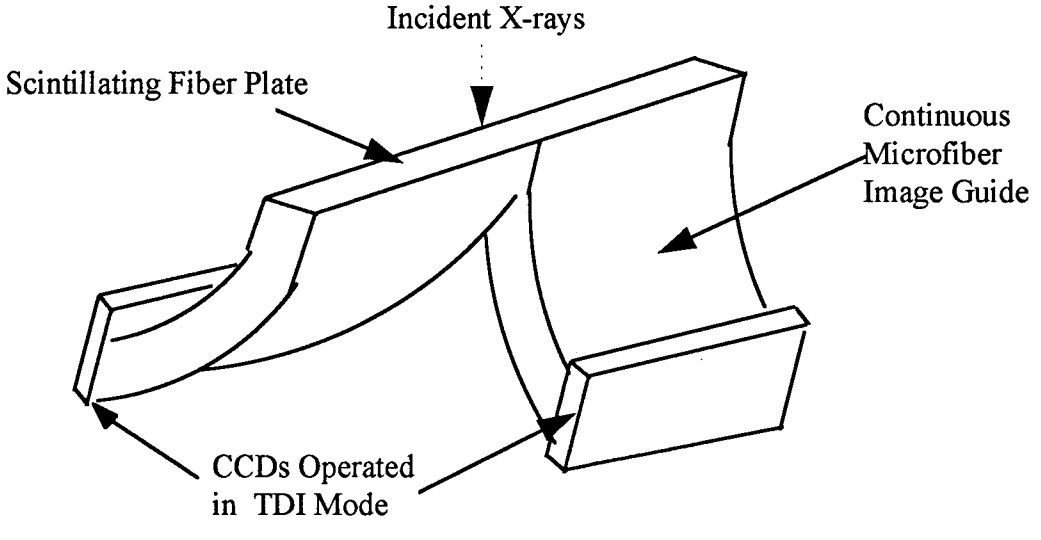

Figure 2. Schematic of the prototype SFP based digital mammography detector.

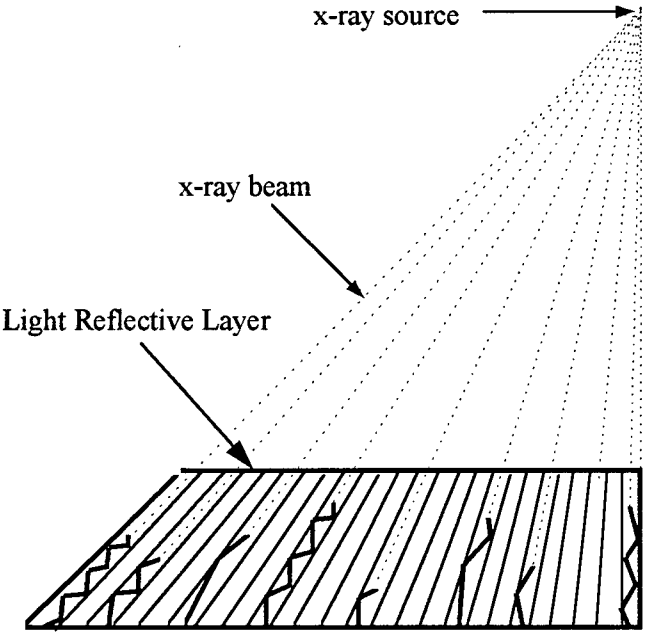

Figure 3. Parallax corrected SFP.

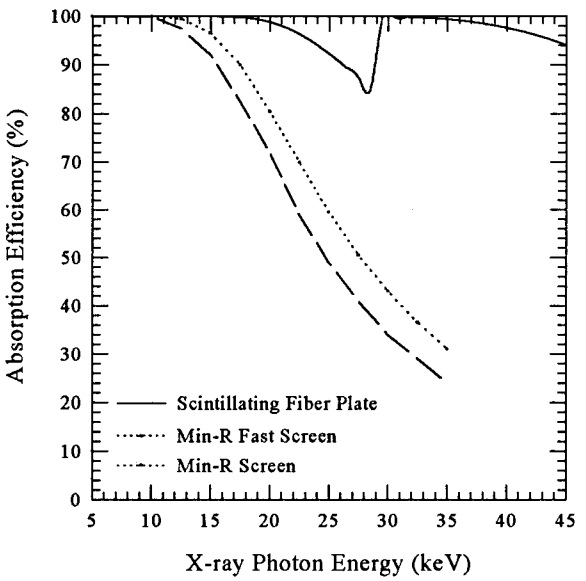

Figure 4. Absorption efficiency of a 2 cm thick, 7.5% tin loaded SFP

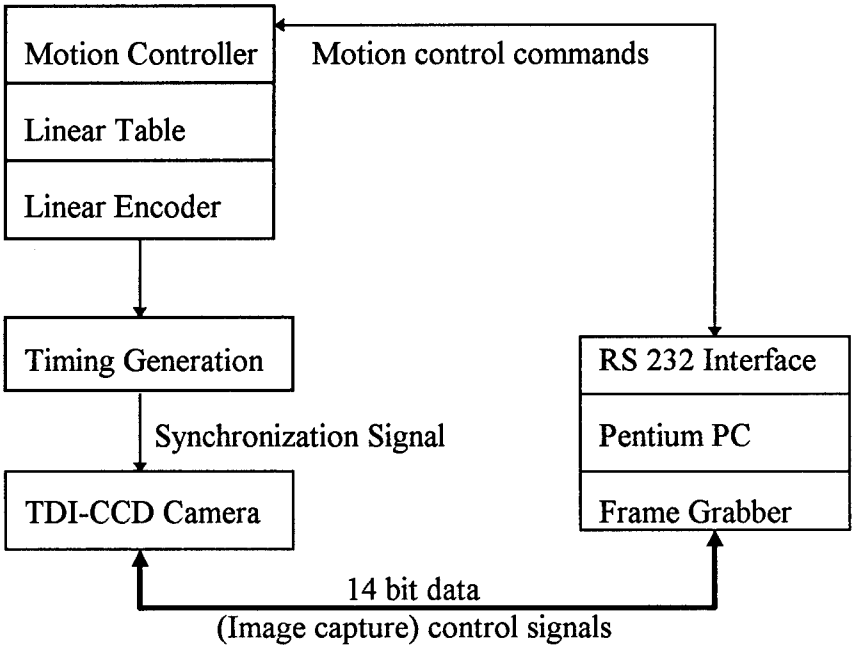

Figure 5. Schematic of the experimental setup

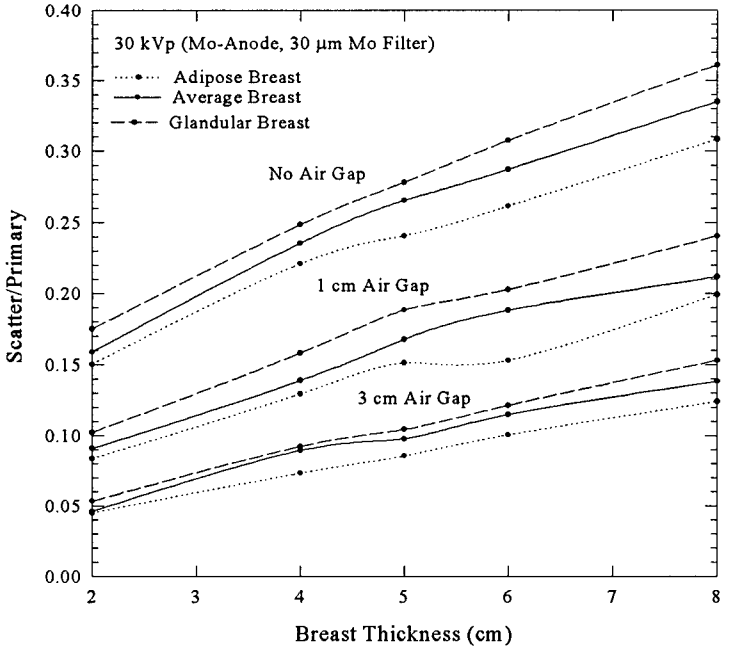

Figure 6. S/P vs. breast thickness for the proposed digital mammography system

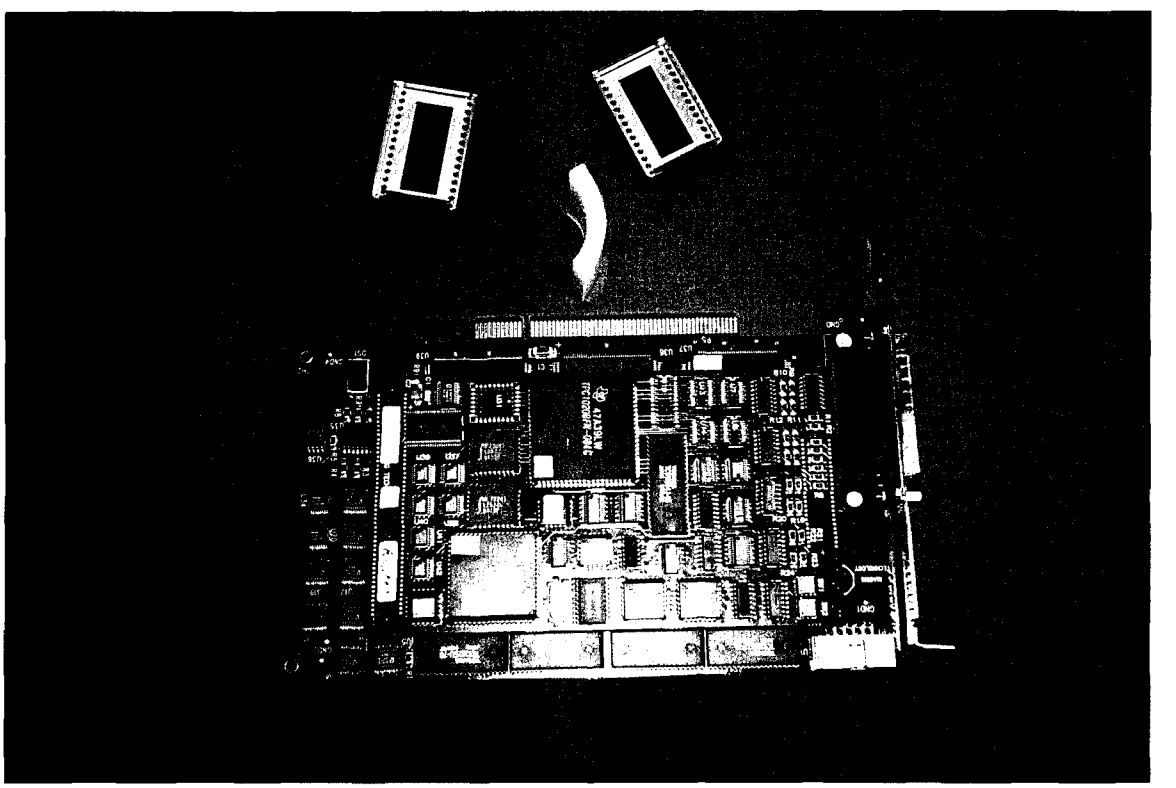

Figure 7. A photograph of one SFP module, two CCDs, and the frame grabber board

Figure 8. A photograph of the mammography x-ray unit and linear scanning table

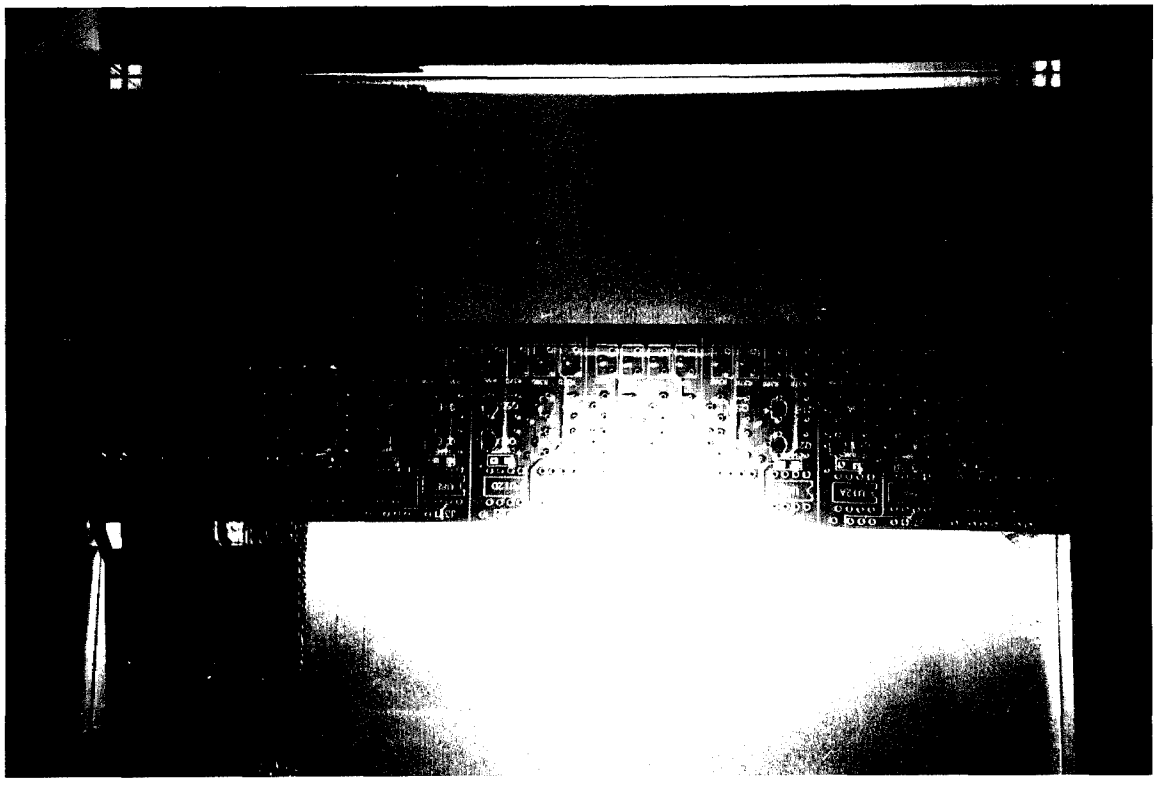

(a)

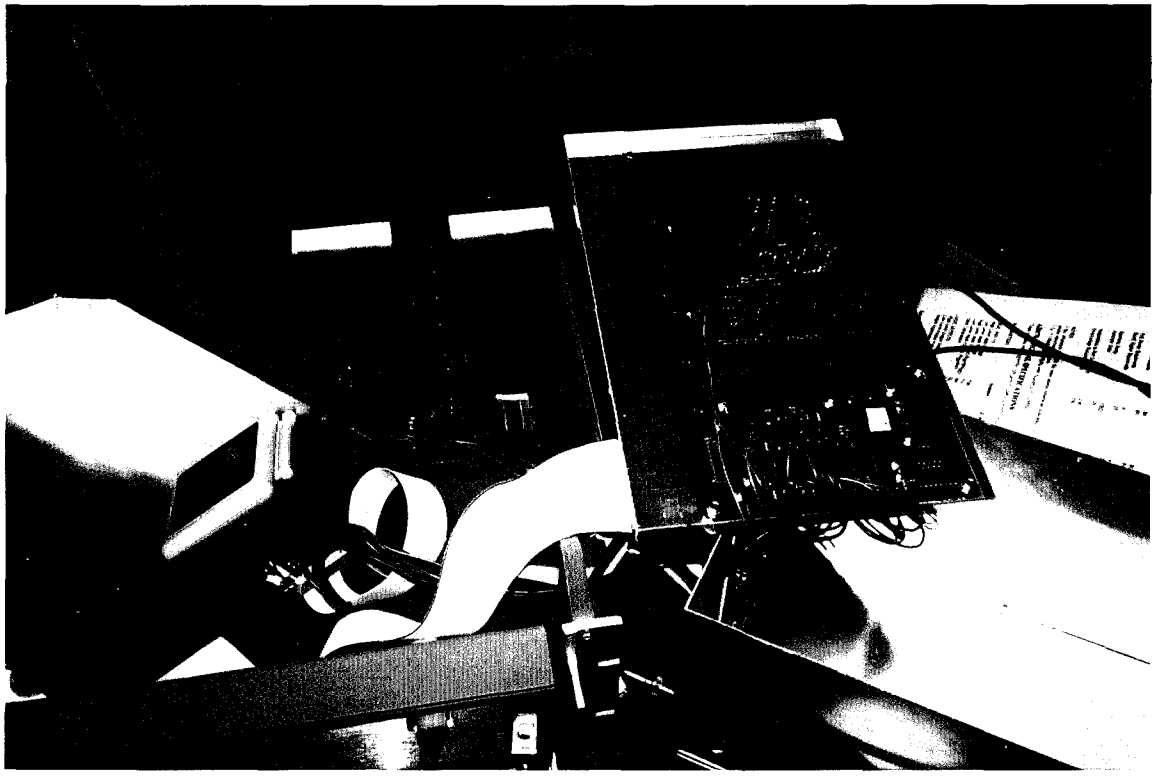

(b)

Figure 9. (a) A photograph of the camera electronics and one CCD module; (b) The box in the right side contains the camera readout unit and one ADC module.

REFERENCES

[1] M. Nishikawa G. E. Mawdsley, A. Fenster and M. J. Yaffe, "Scanned-projection digital mammography", Med. Phys. 14, 5, 717-727 (1987).

[2] Kuhn and W. Knupfer, "Imaging characteristics of different mammographic screens," Med. Phys. 19 (2) 449-457 (1992)

[3] M. Nishikawa and M. J. Yaffe, "Signal-to-noise properties of mammographic film-screen systems", Med. Phys. 12(1), 32-39 (1985)

[4] G.T. Barnes, I. A. Brezovich "The intensity of scattered radiation in mammography", Radiology **126**, 1978, 243-247

[5] G.R. Hammerstein, D.W. Miller, D.R. White, M.E. Masterson, H.Q. Woodard, J.S. Laughlin, "Absorbed Radiation Dose in Mammography", Radiology, 130: 485-491 (1979)

[6] W. Huda, A.M. Sourkes, J.A. Bews, R. Kowaluk, "Radiation Doses Due to Breast Imaging in Manitoba: 1978-1988", Radiology 1990; 177: 813-816

[7] R. Dance, J. Persliliden, G. A. Carlsson "Calculation of dose and contrast for two mammographic grids", Phys. Med. Biol., 1992, Vol. 37, No. 1, 235-248

[8] Gary T. Barnes, "Mammography Equipment: Compression, Scatter Control, and Automatic Exposure Control", Syllabus: *A Categorical Course in Physics Technical Aspects of Breast Imaging* Ed. by A.G. Haus and M.J. Yaffe, RSNA Publications, Oakbrook, Il, 59-68 (1992)

[9] H. Chan, C. J. Vyborny, H. MacMahon, C. E. Metz, K. Doi, E. A. Sickles, "Digital Mammography: ROC Studies of the Effect of Pixel Size and Unsharp-Mask Filtering on the Detection of Subtle Microcalcifications", Investigative Radiology, Vol. 22, No. 7, 581-589 (1987)

[10] N. Karssemeijer, J.T.M. Frieling, J.H.C.L. Hendriks, "Spatial Resolution in Digital Mammography", Investigative Radiology, Vol. 28, No. 5, 413-419 (1993)

[11] H. Chan, L.T. Niklason, D.M. Ikeda, K.L. Lam, "Digitization requirements in mammography: Effects on computer-aided detection of microcalcifications", Med. Phys 21(7), 1203-1211 (1994)

[12] Gambaccini, M. Marziani, O. Rimondi "Phantoms and dynamic range in mammography", Radiation Protection Dosimetry, Vol. 49, Nos 1/3, pp 187-191 (1993)

[13] Maidment, R. Fahrig, M. J. Yaffe "Dynamic range requirement in digital mammography", Med. Phys., 20(6), Nov/Dec, 1993, 1621-1633.

[14] Piccaro and E. Toker, "Development and evaluation of a CCD-based digital imaging system for mammography", in Electronic Imaging. SPIE X (Feb. 1993)

[15] A. Karellas, L.J. Harris, "Charge-coupled device detector: Performance considerations and potential for small-field mammographic imaging applications", Med. phys., 19(4), 1015-23 (1992)

[16] R. Fahrig, J.A. Rowlands, M.J. Yaffe, "X-ray imaging with amorphous selenium: Detective quantum efficiency of photoconductive receptors for digital mammography", Med. Phys. 22(2), 153-160 (1995)

[17] A.D.A. Maidment, M.J. Yaffe, D.B. Plewes, G.M. Mawdsley, I.C. Soutar, B.G. Starkoski, "Imaging performance of a prototype scanned-slot digital mammography system", Proc. SPIE 1896, 93-103 (1993)

[18] U. Neitzel, I. Maack, SG Kohfahl, "Image quality of a digital chest radiography system based on a selenium detector", Med. phys., 21(4), 509-16 (1994)
[19] HG Chotas, CE Floyd, Jr, CE Ravin, "Technical Evaluation of a Digital Chest Radiography System That Uses a Selenium Detector", Radiology 1995; 195:264-270.
[20] P.C. Bunch, "Detective quantum efficiency of selected mammographic screen-film combinations", SPIE Vol. 1090, 67-77 (1989)
[21] Gluer, W.R. Dix, W. Graeff, W. Kupper and K.H. Stellmaschek, "A fast low-noise line scan x-ray detector," Med. Phys. 16(1), pp 98-104 (1989)
[22] W. Y.Choi, Z. Jing, J. K Walker, "A high resolution digital x-ray imaging system based on scintillating plastic microfiber technology", SPIE Vol. 2163, Physics of Medical Imaging, 150-157 (1994)
[23] W. Qian, L. Clark, "Adaptive multiple nonlinear filter and wavelets for the enhancement of medical image", Abstract, Med. Phys 22(6), 989 (1995)
[24] D.R. Dance, G.J. Day, "Escape probabilities for fluorescent x-rays", Phys. Med. Biol., 1985, Vol. 30, No. 3, 259-262
[25] B.A. Arnold, B.E. Bjarngard, "The effect of phosphor K x-rays on the MTF of rare-earth screens", Med. Phys. 6(6), 500-503 (1979)
[26] H. Chan, K. Doi, "Energy and angular dependence of x-ray absorption and its effect on radiographic response in screen-film systems", Phys. Med. Biol., 1983, Vol. 28, No. 5, 565-579
[27] R. Morlotti, "X-ray efficiency and modulation transfer function of fluorescent rare earth screens, determined by the Monte Carlo method", J. Phot. Sci. 23, 181-189 (1975)
[28] J. H. Hubbell, "Bibliography and current status of K, L, and higher shell fluorescence yields for computations of photon energy-absorption coefficients", US Dept. of Commerce, NISTIR 89-4144 (1989)
[29] G. Rakavy, A. Ron, "Atomic Photoeffect in the Range E_γ = 1-2000 keV", Physical Review, Vol. 159, No. 1, 50-56 (1967)
[30] H. Brysk, C.D. Zerby, "Photoelectric Cross Sections in the keV Range", Physical Review, Vol. 171, No. 2, 292-298 (1968)
[31] H. Wong, Y.L. Yao, and E.S. Schlig, "TDI charge-coupled devices: Design and applications," IBM J. Res. Develop, Vol 36 No.1, 83-106 (1992)
[32] Holdsworth, R.K. Gerson, and A. Fenster, "A time-delay integration charge-coupled device camera for slot-scanned digital radiography," Med. Phys. 17 (5), 876-886 (1990)
[33] M.M. Blouke, J.R. Janesick, T. Elliot, J.E. Hall, M.W. Cowens, P.J. May, "Current sataus of the 800 x 800 charge-coupled-device image sensor", Opt. Eng. 26, 864-874 (1987)
[34] M.V. Yester, G.T. Barnes, M.A. King, "Experimental measurements of the scatter reduction obtained in mammography with a scanning multiple slit assembly", Med. Phys. 8, 158-162 (1981)
[35] Z. Jing, W. Huda, J. K. Walker, "Scattered radiation in mammography using a scanning slot detector", To be presented at 1995 RSNA annual meeting, Nov., 1995, Chicago.

[36] T.R. Fewell, R.E. Shuping, Handbook of Mammographic X-ray Spectra, DHEW Publ. (FDA) 79-8071 (U.S. GPO, Washington, D.C., 1978)

[37] S.E. Skubic, P.P. Fatouros, "The effect of breast composition on absorbed dose and image contrast", Med. Phys. 16(4), 544-552 (1989)

[38] R. Fahrig, J. G. Mainprize, N. Robert, A. Rogers, M. J. Yaffe, "Performance of glass fiber antiscatter devices at mammographic energies", Med. Phys., 21(8), 1277-1282 (1994)